Research Square

Preprints are preliminary reports that have not undergone peer review.
They should not be considered conclusive, used to inform clinical practice,
or referenced by the media as validated information.

Geomorphic calibration of friction and entrainment parameters for a snowmelt-induced muddy debris flow in the Longiarù Valley, Dolomites

Litan Dey

litanwre@gmail.com

National Institute of Technology Agartala https://orcid.org/0000-0002-3101-4830

Francesco Comiti

University of Padova: Universita degli Studi di Padova

Martin Mergili

TU Graz: Technische Universitat Graz

Pierpaolo Macconi

Autonomous Province of Bozen/Bolzano: Provincia autonoma di Bolzano - Alto Adige

Marco Cavalli

Institute of Geosciences and Earth Resources National Research Council Padua Branch: Istituto di Geoscienze e Georisorse Consiglio Nazionale delle Ricerche Sede Secondaria di Padova

Stefano Crema

Institute of Geosciences and Earth Resources National Research Council Padua Branch: Istituto di Geoscienze e Georisorse Consiglio Nazionale delle Ricerche Sede Secondaria di Padova

Eleonora Dallan

University of Padova: Universita degli Studi di Padova

Volkmar Mair

Autonomous Province of Bozen/Bolzano: Provincia autonoma di Bolzano - Alto Adige

Lukas Patscheider

Graz University of Technology: Technische Universitat Graz

Marco Borga

University of Padova: Universita degli Studi di Padova

Research Article

Keywords: Snowmelt-induced debris flow, friction parameter calibration, turbulent friction, entrainment, DEM of Difference (DoD)

Posted Date: November 6th, 2026

DOI: https://doi.org/10.21203/rs.3.rs-11390146/v1

License: This work is licensed under a Creative Commons Attribution 4.0 International License.
Read Full License

Geomorphic calibration of friction and entrainment parameters for a snowmelt-induced muddy debris flow in the Longiarù Valley, Dolomites

Litan Dey[1], Francesco Comiti[2], Martin Mergili[3], Pierpaolo Macconi[4], Marco Cavalli[5], Stefano Crema[5], Eleonora Dallan[2], Volkmar Mair[6], Lukas Patscheider[7], and Marco Borga[2*]

[1]Department of Civil Engineering, National Institute of Technology, Agartala, India
[2]Department of Land Environment, Agriculture and Forestry, University of Padova, Padua, Italy
[3]University of Graz, Department of Geography and Regional Science, Graz, Austria
[4]Civil Protection Agency, Autonomous Province of Bozen-Bolzano, Bolzano, Italy
[5]Institute of Geosciences, National Research Council, Padua, Italy
[6]Geological Survey, Autonomous Province of Bozen-Bolzano, Bolzano, Italy
[7]Institute of Soil Mechanics, Foundation Engineering and Numerical Geotechnics, Graz University of Technology, Graz, Austria

Abstract

Snowmelt- and rainfall-triggered debris flows are important geomorphic hazards in alpine environments, yet frictional and entrainment parameters are rarely available for individual events. This study constrains these parameters for a snowmelt-induced muddy debris flow that occurred in the Seres Creek catchment, Longiarù Valley, Dolomites, on 17–18 June 2024. A pre-event DEM from 2010 and a post-event LiDAR-derived DEM from 2024 were used to derive a DEM of Difference (DoD) and characterize the spatial distribution of erosion and deposition associated with the event. The observed geomorphic response was then used to constrain the internal friction, basal friction, turbulent friction, and entrainment parameters through iterative r.avaflow simulations. The calibrated parameter combination comprised an internal friction angle of 17°, a basal friction angle of 9°, a turbulent friction parameter of 10 m/s², and an entrainment coefficient of $10^{-5.55}$ kg⁻¹. The resulting simulation reproduced the major spatial characteristics of the observed event, including the transition from erosion and channel incision in the upper and intermediate reaches to deposition downstream. Comparisons of selected turbulent friction and entrainment values showed that turbulent friction strongly affected flow mobility, erosion, and runout, whereas entrainment substantially influenced flow momentum, erosion, and the downstream position of deposition. Comparison of simulated and DoD-derived geomorphic changes along the main flow path and at three representative cross-sections showed good spatial agreement in the major erosion–deposition patterns, with relatively minor localized differences in erosion and deposition magnitude. The results show that spatially distributed geomorphic change can provide constraints on frictional and entrainment parameters beyond runout extent alone, providing a spatially informed basis for event-scale debris-flow modelling.

Keywords: Snowmelt-induced debris flow; friction parameter calibration; turbulent friction; entrainment; DEM of Difference (DoD).

Introduction

1. Introduction

Debris flows are rapid, gravity-driven mixtures of sediment and water that pose substantial hazards to mountain communities and infrastructure (Varnes, 1978; Jakob & Hungr, 2005; Iverson, 2014). In alpine environments, snowmelt combined with rainfall can rapidly mobilize unconsolidated material on steep slopes, generating highly mobile flows (Takahashi, 2009; Simoni et al., 2020). The Dolomites in the eastern Italian Alps are particularly susceptible to debris flows because of their steep terrain, complex geology, and pronounced seasonal hydrological variability (Dallan et al., 2025). Snowmelt-induced debris flows are of particular concern because variations in snowpack conditions and runoff generation can influence the timing and magnitude of sediment mobilization (Borga et al., 2014; Stoffel et al., 2014). Once initiated, debris-flow behaviour is governed by the interaction between material properties, flow resistance, and entrainment of bed material, which together influence flow mobility, erosion, and deposition (Iverson, 1997; Hungr et al., 2014). Representing these processes numerically remains challenging because key frictional and entrainment parameters are rarely measured directly for individual events (Pastor et al., 2009; Mergili et al., 2017).

This difficulty is particularly relevant to muddy debris flows, for which high water content, fine-grained material, and strong sediment–fluid interactions can produce complex and spatially variable flow behaviour (Berti & Simoni, 2005; Tiranti et al., 2019). Frictional and entrainment parameters may also vary considerably between events and catchments, making their calibration an important source of uncertainty in physically based simulations (Frank et al., 2015). In practice, model calibration is often constrained by bulk characteristics of an event, such as runout extent or deposit distribution. These characteristics are important, but they provide limited information on how erosion and deposition vary along the flow path. Additional spatially distributed observations are therefore useful for assessing whether a model reproduces not only where the flow travelled, but also how sediment was removed, transported, and deposited during the event.

The increasing availability of high-resolution airborne LiDAR provides an opportunity to quantify these geomorphic changes at the event scale. Repeat topographic surveys can be used to derive DEMs of Difference (DoD) and geomorphic change detection (GCD) products that describe the spatial distribution of erosion and deposition and allow sediment budgets to be estimated (Wheaton et al., 2010; Cavalli et al., 2017; Baggio et al., 2021). Such observations provide a spatially explicit record of geomorphic change that can be compared with simulated erosion and deposition. Previous studies have demonstrated the value of combining DoD-derived geomorphic observations with numerical modelling to investigate debris-flow erosion and entrainment (Dietrich & Krautblatter, 2019; Gregoretti et al., 2019). Integrating these observations with physically based modelling therefore provides an opportunity to constrain model parameters when direct measurements of flow resistance and entrainment properties are unavailable.

Physically based two-phase flow models provide a framework for linking the observed geomorphic response to debris-flow dynamics. Among these, r.avaflow represents interacting solid and fluid phases and allows erosion, entrainment, transport, and deposition to be simulated within a spatially distributed modelling framework (Pudasaini & Mergili, 2019; Mergili et al., 2025). The model incorporates different components of flow resistance, including internal friction, basal Coulomb

friction, and turbulent or velocity-dependent resistance. Together with the rate of bed-material entrainment, these components influence flow mobility and the resulting erosion–deposition pattern (Cuomo et al., 2014; Frank et al., 2015). The two-phase formulation therefore provides a suitable framework for examining how combinations of resistance and entrainment parameters reproduce the geomorphic response of an individual debris-flow event.

Despite these developments, an important challenge remains: how can spatially distributed geomorphic change be used more effectively to constrain the combination of frictional and entrainment parameters in an event-scale debris-flow simulation? Calibration based mainly on bulk characteristics such as runout extent may provide limited information on how well a model reproduces the spatial transition from erosion and channel incision to downstream deposition. The 2010 pre-event DEM and 2024 post-event LiDAR-derived DEM provide an opportunity to use this event-scale geomorphic response as an additional constraint on model calibration. In this study, the observed spatial pattern of event-related geomorphic change is used as a reference for constraining the frictional and entrainment parameters of a two-phase debris-flow model. The approach is applied to the June 2024 snowmelt-induced muddy debris flow in the Seres Creek catchment, with particular emphasis on identifying a parameter combination that reproduces the observed erosion–deposition pattern and examining the influence of turbulent friction and entrainment on the simulated flow dynamics.

This study applies this approach to the snowmelt-induced muddy debris flow that occurred in the Seres Creek catchment, Longiarù Valley, Dolomites, Italy, on 17–18 June 2024. A pre-event DEM from 2010 and a post-event LiDAR-derived DEM from 2024 are used to characterize event-related geomorphic change through DEM of Difference (DoD) and geomorphic change detection (GCD) analyses. These observations are then used to constrain the internal friction, basal friction, turbulent friction, and entrainment parameters of a two-phase r.avaflow model. The calibrated parameter combination is subsequently used to evaluate the event-scale erosion and deposition dynamics and the effects of turbulent friction and entrainment on flow behaviour. In addition to runout extent, the model assessment considers the longitudinal distribution of erosion and deposition and geomorphic changes at three representative cross-sections along the flow path.

The main objectives of this study are to:

1. Quantify the spatial distribution and volume of erosion and deposition associated with the 2024 debris-flow event using DoD and GCD analyses;
2. Constrain the internal friction, basal friction, turbulent friction, and entrainment parameters of a two-phase r.avaflow model by comparing simulated flow behaviour and erosion–deposition patterns with the observed geomorphic response;
3. Assess how the calibrated parameter combination reproduces the event-scale flow dynamics and spatial transition from erosion and channel incision to downstream deposition, and examine the influence of turbulent friction and entrainment on the simulated response.

The study therefore uses the observed geomorphic response of the Longiarù event to identify site-specific frictional and entrainment parameters for r.avaflow simulations. The calibrated model is then used to examine the influence of turbulent friction and entrainment on flow mobility, erosion, and

deposition. The results provide event-specific constraints on model parameters and an assessment of their influence on the simulated geomorphic response.

2. The June 2024 Longiarù debris flow

2.1 Study Site

The Seres Creek catchment (46°36′N, 11°43′E) is situated in the upper Longiarù Valley of South Tyrol, within the north-eastern Dolomites of Italy (Fig. 1a). The area lies within the Southern Limestone Alps and is characterized by complex stratigraphy, steep topography, and active geomorphic processes. The catchment is characterized by rugged terrain, with slope gradients frequently exceeding 25°, and a confined headwater drainage network that provides favorable conditions for sediment accumulation, rapid runoff, and mass-wasting processes. A three-dimensional view of the catchment and the main debris-flow corridor is shown in Fig. 1b, while the post-event orthophoto in Fig. 1c illustrates the mapped study area and debris-flow path.

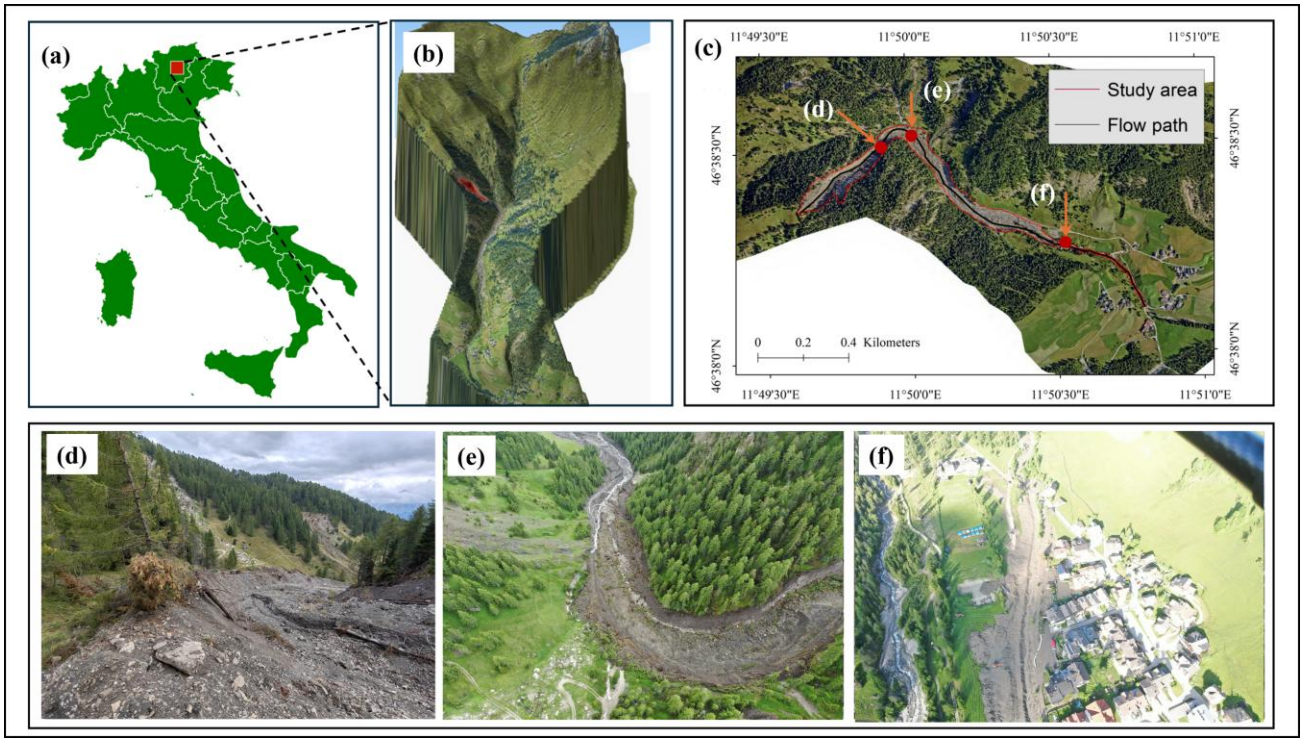


Figure 1: Location and overview of the June 2024 debris-flow event in the Seres Creek catchment, Longiarù Valley, South Tyrol, Dolomites: (a) location of the study area within Italy; (b) 3D perspective view of the Seres Creek catchment showing the debris-flow initiation area and downstream flow corridor; (c) post-event aerial orthophoto showing the study-area boundary and mapped debris-flow path, with red markers indicating the locations of the photographs shown in panels (d–f); (d) field photograph of the debris-flow channel and eroded source/transport area; (e) aerial photograph showing the sharp bend where the debris-flow channel joins the Seres Creek channel and associated channel incision; and (f) aerial view of the downstream deposition area and affected settlement.

Geologically, the study area is situated within the Triassic stratigraphic sequences of the Western Dolomites, comprising mainly dolomite, limestone, siliciclastic, and volcanoclastic units (Fig. 2). The debris flow originated from an approximately 400 m long, colluvium-filled headwater gully without vegetation cover, located southwest of Seres Creek. The source area is situated on an N-fold limb between an anticline and a syncline, with bedding dipping northward at approximately 35–45°. The thin Schlerndolomite forms a dip slope on the SE side of the Ciancidel channel, whereas the Zoppé Formation on the NW side forms an anti-dip slope (Fig. 2). This contrasting lithological setting favors preferential weathering of the mechanically weaker Zoppé Formation and the accumulation of metre-thick regolith and colluvial material within the source area. These geological conditions provided a substantial volume of unconsolidated material susceptible to saturation and subsequent mobilization during the event.

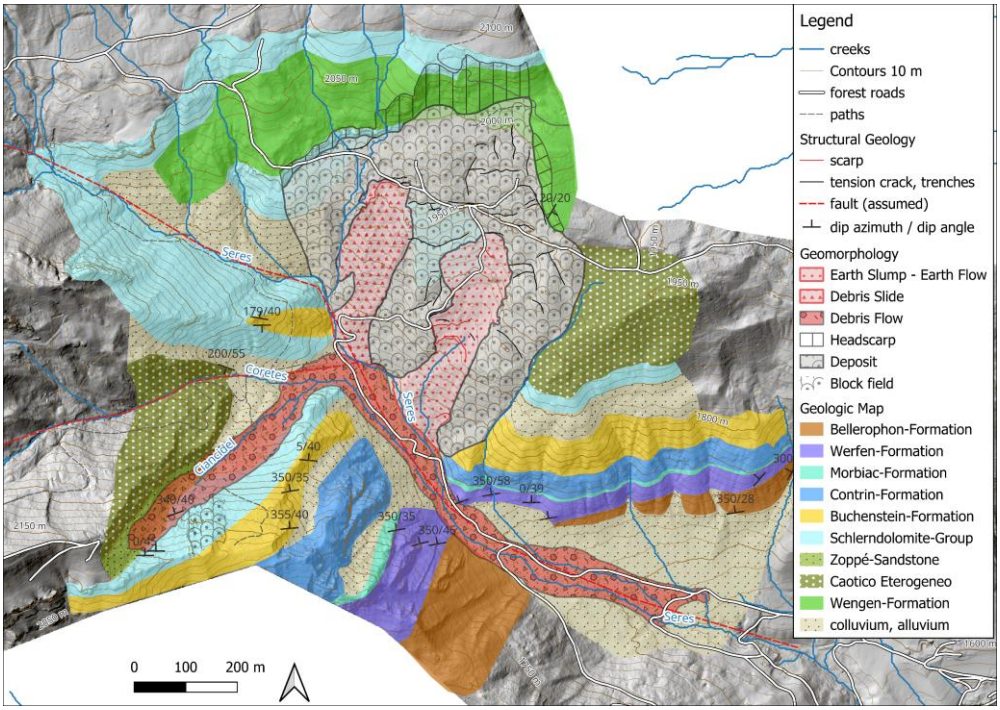


Figure 2: Geological setting of the study area showing the main lithological and structural features of the debris-flow source area.

Topographically, the upper portion of the study area contains several concave hollows and slope breaks that act as natural accumulation zones for snow and colluvium. The channel network becomes progressively more confined downstream, with average slopes ranging from 25° to 38° in the initiation area before flattening toward the deposition fan (Fig. 3). Airborne LiDAR data reveal an intricate drainage structure that facilitates rapid runoff and sediment transfer, which are important preconditions for debris-flow initiation. The Longiarù Valley has a subalpine, cold, and wet climate (Köppen–Geiger DFC), characterized by long winters and substantial snow accumulation, followed by a relatively short but intense snowmelt period during late spring and early summer. Mean annual precipitation is typically around 1,000–1,200 mm (Crespi et al., 2021), with late-spring snowmelt often enhanced by rainfall events that accelerate surface runoff and soil saturation.

2.2 The 2024 debris flow event

During 17–18 June 2024, a complex debris-flow event occurred in the upper Seres Creek catchment following several weeks of above-average spring temperatures, progressive snowmelt, and intermittent rainfall. Antecedent snowmelt and rainfall progressively saturated the near-surface colluvial deposits, triggering failure within a confined headwater gully. The initial slope failure evolved into an earth–debris flow and subsequently into a muddy debris flow through entrainment of stream water and unconsolidated sediments during downstream propagation, before depositing material in the lower valley (Fig. 1c–f).

The debris flow initiated at approximately 1970 m a.s.l. within a confined headwater gully and propagated downslope through an increasingly confined channel system (Fig. 3a,b). Pronounced channel incision occurred along the upper and middle reaches, followed by deposition where the channel gradient decreased. The main deposition area was located at approximately 1670 m a.s.l., while a subsequent mudflow phase continued downstream toward Campill village across lower-gradient terrain (Fig. 1c,e,f). The debris material consisted mainly of fine-grained silty mud with embedded coarse clasts derived from the surrounding dolomitic bedrock.

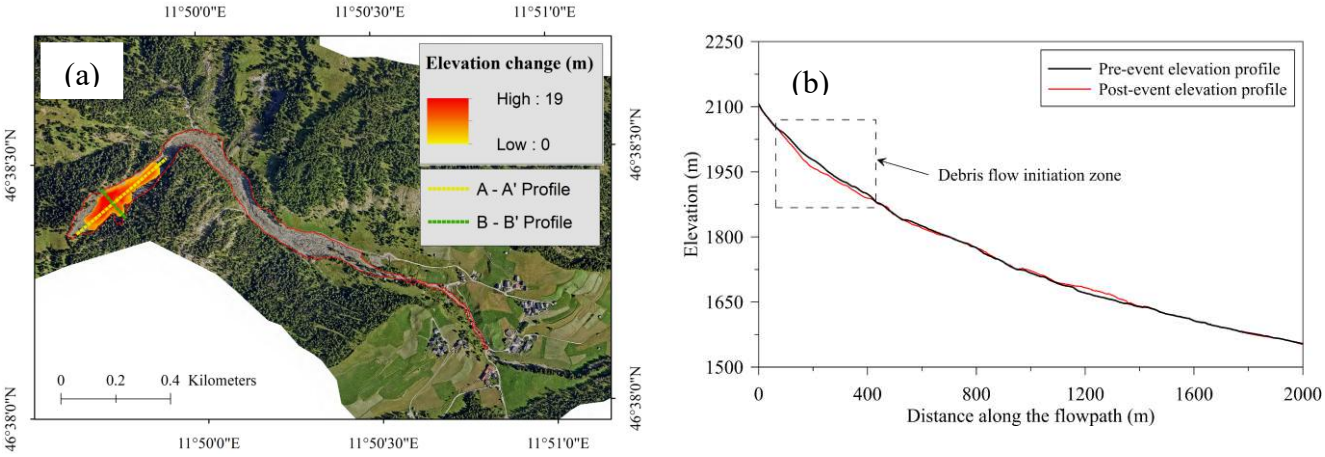


Figure 3: (a) Post-event orthophoto of the Seres Creek catchment (17-18 June 2024) showing the debris-flow channel, deposition fan, and the impact area outlined by a red line. The initial mass-release area is also outlined within this impact region and served as the primary source for the r.avaflow simulations, and (b) Comparison of pre-event (2010) and post-event (2024) elevation profile highlighting the zone of initial mass release

The debris flow originated from an approximately 400 m long, colluvium-filled headwater gully located southwest of Seres Creek. The confined source area is characterized by steep slopes and is bounded by dolomitic bedrock on one side and calciturbidites and siltstones of the Zoppé Formation on the other. The topographic profile along section A–A′ (Fig. 4b) illustrates the elevation and thickness of the source material, while section B–B′ (Fig. 4c) shows the width and depth of the source area at the marked location in Fig. 4a. Figure 4 therefore illustrates the topographic setting and geometry of the material involved in the initial failure.

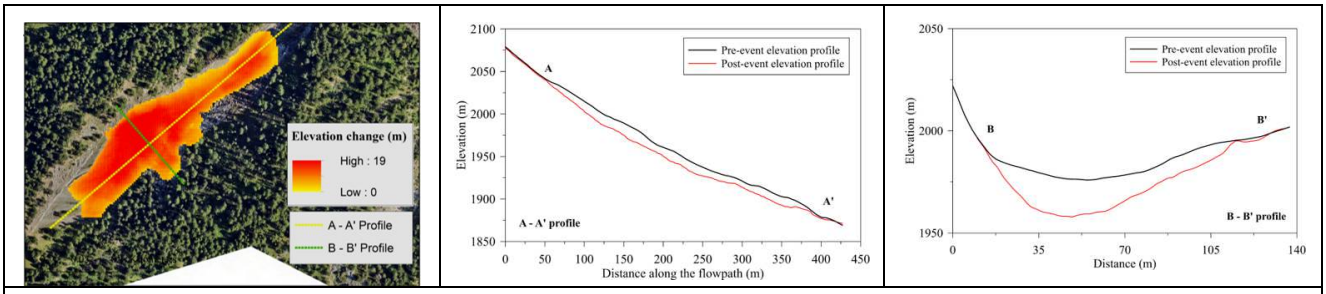


Figure 4. Topographic and geomorphic setting of the debris-flow source area in the upper Seres Creek catchment: (a) 2024 post-event topography showing the headwater gully and source area; (b) topographic profile along section A–A′; and (c) topographic profile along section B–B′.

3. Methodology

3.1 DoD and GCD

Two high-resolution Digital Elevation Models (DEMs) of the Longiarù valley were used to assess topographic changes: a pre-event DEM from 2010 and a post-event LiDAR-derived DEM from 2024. These datasets provided the basis for geomorphic change detection using the DEM of Difference (DoD) method. Both DEMs were resampled onto a consistent 2.5 m resolution grid with linear interpolation to ensure spatial coherence and minimize interpolation artifacts. The pre-processing included error filtering and co-registration to remove systematic misalignments that might skew volume estimations. A preliminary comparison between the 2010 and 2024 DEMs of the Longiarù catchment was carried out using the Change Vector Analysis (CVA) tool available in the open-source GIS WhiteboxTools 2.0.2. This tool enables the calculation of both the magnitude and direction of topographic changes by subtracting the two DEMs. The magnitude layer highlights the amount of elevation change between the two dates, while the directional layer differentiates between erosion and deposition trends.

While this initial comparison effectively visualized patterns of geomorphological change across the catchment, the results were subject to typical sources of error inherent to LiDAR data, including vertical and horizontal inaccuracy as well as differences in the classification and filtering of vegetation or surface structures between the two datasets (Cavalli & Tarolli, 2011). To reduce the influence of these inaccuracies, error propagation was considered, and only the areas exhibiting significant morphologic variation were retained for further DoD analysis. These areas were identified based on the combined interpretation of the CVA magnitude and direction of variation maps, allowing for a spatial focus on geomorphologically active zones. Given the lack of original point-cloud data for the input datasets, uncertainty in the DoD was assessed using the vertical uncertainty assigned to the input DEMs. A uniform vertical uncertainty of ±0.4 m was assigned to both the pre- and post-event DEMs, which is consistent with the expected accuracy of airborne DoD-derived DEMs in alpine terrain. Following Brasington et al. (2000) and Wheaton et al. (2010), the propagated vertical uncertainty of the DoD was calculated as:

$$\delta_{DoD} = \sqrt{\left(\delta_{z_{2024}}\right)^2 + \left(\delta_{z_{2010}}\right)^2} \quad (1)$$

where δ_{DoD} is the total propagated vertical uncertainty, $\delta_{z_{2024}}$ and $\delta_{z_{2010}}$ are the vertical uncertainties of the 2024 and 2010 DEMs, respectively. A uniform vertical uncertainty of ±0.4 m was assigned to both the pre- and post-event DEMs based on the available data accuracy information.

The final analysis of surface change in the Longiarù catchment was performed using the Geomorphic Change Detection (GCD) software, version 5, implemented as a plugin for ArcGIS (Wheaton et al., 2010). GCD provides a framework for calculating elevation differences between DEMs while accounting for uncertainty in the input data. Although the software supports spatially variable error models based on metrics such as point density, scan angle, and surface roughness, these could not be applied in our case because the original LiDAR point clouds were unavailable. Therefore, two simplified uncertainty approaches were considered: the Minimum Level of Detection (minLoD) method (Brasington et al., 2000; Fuller et al., 2003) and the probabilistic thresholding method based on a 95% confidence interval (Anderson, 2019). For the minLoD approach, both DEMs were assigned a uniform vertical uncertainty of ±0.4 m. For the probabilistic approach, a 95% confidence level was applied, retaining elevation changes with $p < 0.05$. The two approaches were evaluated and the probabilistic thresholding approach was selected for the final DoD analysis because it produced less noise while retaining meaningful topographic changes. This approach was therefore used to distinguish statistically significant elevation changes from differences that could arise from uncertainties in the DEMs, providing a cleaner and more interpretable delineation of erosion and deposition zones (Brasington et al., 2003).

3.2 Numerical method

The snowmelt-induced debris flow was simulated using the open-source mass-flow simulation framework r.avaflow v4.0, implemented within GRASS GIS 8.4.1 (Mergili et al., 2025). r.avaflow is a GIS-based numerical modelling framework developed to simulate gravitational mass flows and related process chains using depth-averaged conservation equations. The current version is derived from the multi-phase modelling framework proposed by Pudasaini and Mergili (2019) and supports simulations involving up to three interacting phases with various rheological formulations. In the present study, the model was applied in a two-phase configuration representing the solid and fluid components of the debris-flow mixture. The governing equations are expressed in a depth-averaged conservative form based on mass and momentum conservation (Pudasaini and Mergili, 2019; Mergili et al., 2025). The mass conservation equation for the solid and fluid phases is written as

$$\frac{\partial}{\partial t}(C_{vs}h) + \frac{\partial}{\partial x}(C_{vs}hu_s) + \frac{\partial}{\partial y}(C_{vs}hv_s) = 0 \quad (2)$$

$$\frac{\partial}{\partial t}\left(C_{vf}h\right) + \frac{\partial}{\partial x}\left(C_{vf}hu_f\right) + \frac{\partial}{\partial y}\left(C_{vf}hv_f\right) = 0 \quad (3)$$

where the subscripts *s* and *f* denote the solid and fluid phases, respectively. The total volumetric concentration can be represented by C_{vt}, where $C_{vt} = C_{vs} + C_{vf} = 1$, C_{vs} and C_{vf} are volumetric concentrations of solids and fluids, respectively. The total flow depth is denoted by h, and u_s, v_s, u_f, and v_f are the depth-averaged flow velocities of the respective phases.

The depth-averaged momentum conservation equations are written as

$$\frac{\partial(\alpha_k h u_k)}{\partial t} + \frac{\partial F_{x,k}}{\partial x} + \frac{\partial G_{x,k}}{\partial y} = S_{x,k} \quad (4)$$

$$\frac{\partial(\alpha_k h v_k)}{\partial t} + \frac{\partial F_{y,k}}{\partial x} + \frac{\partial G_{y,k}}{\partial y} = S_{y,k} \quad (5)$$

where $k = s$ and $k = f$ denote the solid and fluid phases, respectively; F and G represent the momentum fluxes, respectively, and S denotes the source terms governing momentum production and dissipation.

Following Mergili et al. (2025), the source terms governing momentum production and dissipation can be represented in generalized form as

$$S = f(GA, DF, DR, EC, FE, TF, FF, AD, VT) \quad (6)$$

where (*GA*) denotes gravitational acceleration, (*DF*) internal deformation, (*DR*) interphase drag, (*EC*) the extended Coulomb friction term, (*FE*) fragmentation and energy-loss effects, (*TF*) turbulent friction, (*FF*) fluid friction, (*AD*) ambient drag, and (VT) viscous stress contributions (Mergili et al., 2025). The detailed mathematical formulation of these terms is provided by Pudasaini and Mergili (2019) and Mergili et al. (2025).

In the adopted two-phase configuration, the solid phase is governed primarily by frictional resistance, whereas the fluid phase is characterized by viscous and turbulent flow behaviour. Interactions between the phases are represented through drag and momentum-transfer mechanisms that influence flow mobility, entrainment, and deposition processes (Pudasaini and Mergili, 2019). The governing equations were solved using a Total Variation Diminishing Non-Oscillatory Central Differencing (TVD-NOC) scheme implemented on a staggered computational grid (Tai et al., 2002; Wang et al., 2004; Mergili et al., 2025).

3.2.1 Model setup, topographic input, and boundary conditions

The r.avaflow model (Mergili et al., 2017, 2025) was employed to simulate the dynamics of the 2024 Seres Creek debris flow using a two-phase mass-flow approach, in which the solid and fluid components are treated as interacting continua. The model solves depth-averaged mass and momentum conservation equations for both phases and allows entrainment and deposition along the flow path. The 2024 post-event LiDAR-derived DEM was used as the basal topography for the simulations. The initial flow-release zone and associated source conditions were defined from the geomorphic evidence described in Section 3.1. The released material was assumed to be fully mobilized at the onset of the simulation, consistent with field observations of a highly saturated, fine-grained debris mixture. An initial release depth of 0.30 m, corresponding to approximately 30% of the estimated available source material, was prescribed as the initial mass input.

The model domain encompassed the entire channel network from the initiation area to the deposition fan and extended slightly beyond the mapped deposition limits to avoid boundary-induced artefacts. No-flow boundary conditions were applied at the lateral margins of the domain, while free-outflow conditions were assigned at the downstream boundary to permit unimpeded discharge. All simulations were performed at a 2.5 m grid resolution with a simulation time step of 0.01 s. The entrainment and deposition routines were activated to account for sediment incorporation and material loss along the channel. Model initialization assumed a hydrostatically distributed velocity field and a uniform

mixture density, consistent with the partially saturated, muddy composition observed in the field. Entrainment was dynamically updated based on local basal shear stress and slope gradients. The simulation period extended until the flow reached a quasi-stationary deposition state, defined by near-zero flow velocity (<0.05 m/s) across the domain. Model outputs included time-dependent flow depth, velocity magnitude, and entrainment–deposition volumes.

3.2.2 Model calibration

Because no field or laboratory measurements of the frictional or entrainment parameters were available for the 2024 event, the model parameters were constrained through an iterative trial-and-error calibration procedure using the DoD-derived geomorphic response as the observational reference. The internal friction angle (δ), basal friction angle (ϕ_b), turbulent friction coefficient (ξ), and entrainment coefficient (C_E) were systematically varied through repeated numerical simulations. During calibration, these parameters were explored over the ranges of 15–30°, 7–15°, 8–20 m/s², and $10^{-5.25} - 10^{-5.75}$ kg⁻¹, respectively. For each simulation, the simulated runout extent, flow depth, deposition thickness, and overall erosion–deposition morphology were compared with the observed geomorphic changes derived from the DoD. The calibration focused on identifying parameter combinations that reproduced the observed runout extent, lateral confinement, and spatial distribution of erosion and deposition associated with the 17–18 June 2024 debris-flow event. The parameter ranges explored during calibration and the final calibrated values are summarized in Table 1. The final calibrated parameter combination was subsequently used for the simulations presented in the Results section.

Table 1. Model parameters used in the r.avaflow v4.0 simulations of the Longiarù debris-flow event

Parameters	Symbols	Parameter ranges	Calibrated values
Solid material density (grain density)	ρ_s (kg/m^3)	2700	2700
Mixture (solid-fluid) material density	ρ_m (kg/m^3)	1800	1800
Fluid material density	ρ_f (kg/m^3)	1000	1000
Solid internal friction angle	δ (°)	$15 - 30$	17
Solid basal friction angle	ϕ_b (°)	$7 - 15$	9
Turbulent friction parameter	ξ (m/s^2)	$8 - 20$	10
Fluid friction number	C_{FF}	0.01	0.01
Entrainment coefficient	C_E (kg^{-1})	$10^{-5.25} - 10^{-5.75}$	$10^{-5.55}$

Representative cross-sections were selected along the debris-flow path to facilitate a spatial comparison between the observed topographic changes derived from the DoD and the simulated response. Three sections were selected based on their distinct geomorphic settings and expected flow behaviour. Section 1 is located immediately downstream of the initiation area and represents the initial propagation stage of the debris flow. Section 2 is located at a pronounced channel bend characterized by strong channel incision and therefore represents a highly erosional and dynamically active reach. Section 3 is located within the downstream deposition fan and represents the transition to deposition

and flow deceleration. These three sections were selected to capture contrasting stages and geomorphic responses along the flow path and to provide representative locations for comparing the observed and simulated elevation changes. The locations of these cross-sections are shown in Fig. 5.

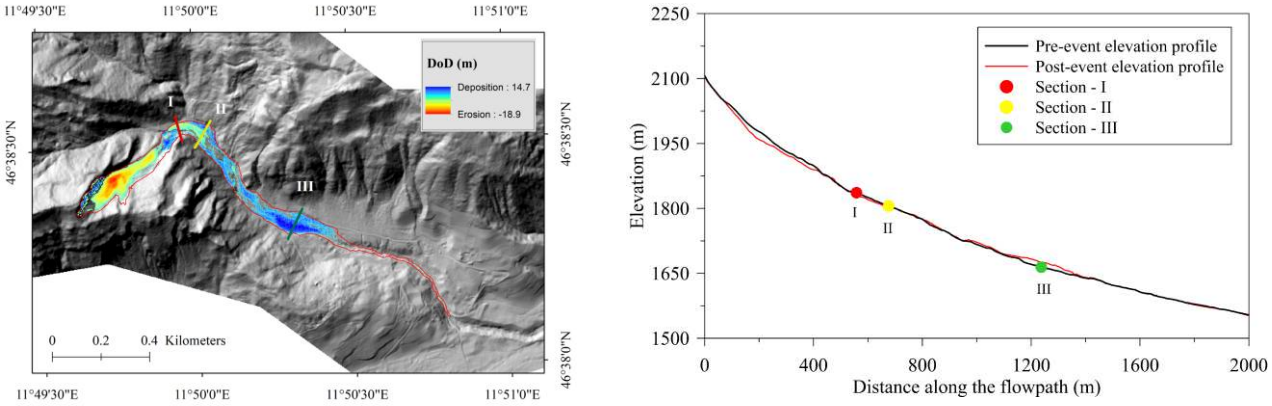


Figure 5: Representative cross-sections selected for comparison between observed and simulated topographic changes along the debris-flow path. Section 1 represents the reach immediately downstream of the initiation area, Section 2 represents the sharp bend and strongly incised channel reach, and Section 3 represents the downstream deposition fan.

4. Results and Discussion

This section first presents the geomorphic changes associated with the 17–18 June 2024 debris-flow event derived from the DoD and GCD analysis. These observations provide the geomorphic reference for the subsequent r.avaflow simulations. The calibrated model results are then presented and evaluated in terms of flow dynamics, erosion and deposition patterns, and their correspondence with the observed topographic changes.

4.1 DEM of Difference (DoD) and Geomorphic Change Detection (GCD) analysis

The DEM of Difference (DoD), derived from the 2010 pre-event DEM and the 2024 post-event LiDAR-derived DEM, was used to characterize the geomorphic response of the 17–18 June 2024 debris flow. Application of the probabilistic thresholding approach at the 95% confidence level isolated elevation changes considered statistically significant relative to the uncertainty of the input DEMs. A uniform vertical uncertainty of ±0.40 m was assigned to each DEM, resulting in a propagated DoD uncertainty of approximately ±0.57 m, following the error-propagation approach described by Brasington et al. (2000) and Wheaton et al. (2010). The use of probabilistic thresholding provides a means of distinguishing meaningful topographic changes from elevation differences associated with DEM uncertainty (Anderson, 2019).

The detected changes can be broadly divided into three geomorphic domains along the flow path (Figs. 6 and 7). In the initiation zone, concentrated within the confined headwater depression, erosion was dominant. The delineated source area experienced a net erosion of approximately 7,100 m^3, with a mean elevation change of about −2.3 m, indicating substantial removal and mobilization of the

colluvial material that formed the initial debris-flow mass. Downstream, within the transport corridor, erosion continued through both channel-bed incision and lateral bank retreat. The total eroded volume within this domain was approximately 11,320 m³, with local elevation changes reaching −4.1 m, particularly along confined channel sections and bends. These changes indicate progressive modification of the channel during debris-flow passage. Further downstream, within the deposition fan, the geomorphic response shifted from erosion to accumulation. Approximately 16,850 m³ of material accumulated, with a mean deposition thickness of about +1.8 m. Deposition became particularly pronounced where the channel gradient decreased to below approximately 12°, promoting reduced flow competence and lateral spreading of the debris.

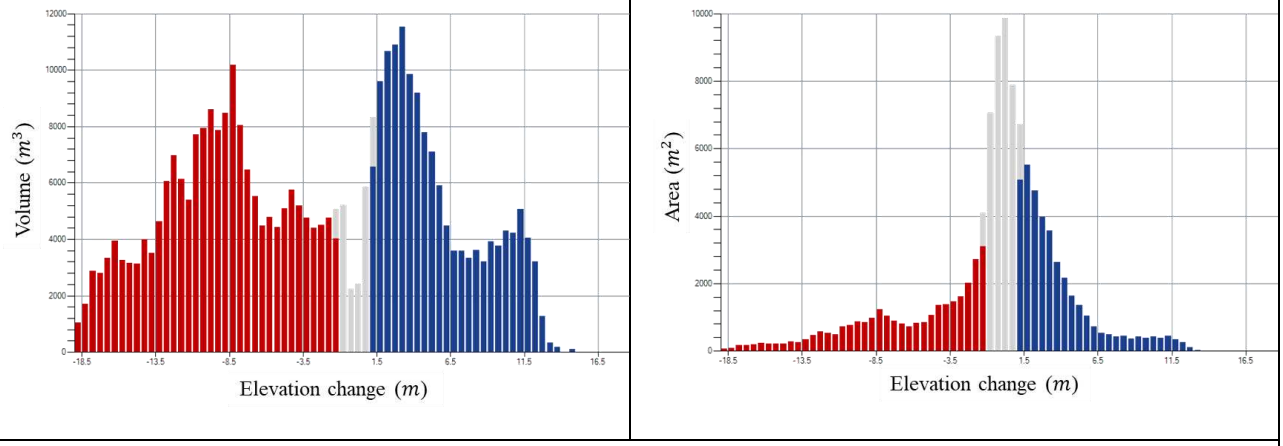


Figure 6: Graphical results of elevation change on the thresholded DoD

The three-domain volume estimates yield a net volumetric deficit of approximately 1,570 m³ when the estimated deposition is compared with the combined erosion within the initiation and transport zones. This difference may reflect sediment remaining outside the delineated domains, export beyond the surveyed or mapped area, or spatial redistribution of material within areas not included in the three-domain accounting. Because the available GCD output provides volumetric uncertainty estimates for the overall area of interest rather than for these three individually delineated geomorphic domains, separate uncertainty bounds are not assigned to the domain-specific volume estimates. The treatment of uncertainty follows established approaches for accounting for DEM errors in geomorphic change and sediment-budget analyses (Brasington et al., 2000; Wheaton et al., 2010).

The elevation-change distributions provide a quantitative overview of the magnitude and spatial extent of surface lowering and raising associated with the event (Fig. 7). Negative elevation changes represent erosion, whereas positive changes represent deposition. Figure 7 spatially resolves these changes along the debris-flow path and illustrates the transition from erosion-dominated conditions in the upper catchment to deposition-dominated conditions downstream. The initiation hollow, with an average slope of approximately 28°, corresponds to the principal source and erosion area. Along the intermediate channel, pronounced erosion occurs at confined reaches and bends, where local elevation differences reach approximately 4.1 m. In contrast, the lower-gradient deposition fan is characterized by positive elevation changes and progressive accumulation of debris. Overall, the DoD results reveal a coherent spatial pattern of geomorphic change, characterized by erosion in the source area, continued

channel incision and bank erosion along the transport corridor, and deposition in the downstream fan. This pattern is consistent with the field observations and highlights the progressive transition from erosion-dominated to deposition-dominated conditions along the debris-flow path.

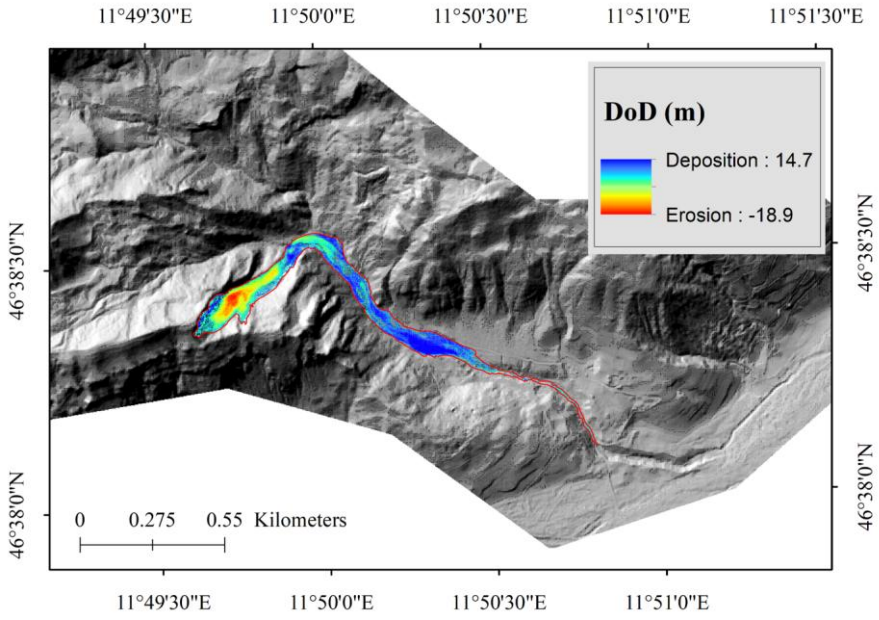


Figure 7: Magnitude of geomorphic change in the Seres Creek

4.2 Model simulation and calibration of the 2024 debris flow

The simulations identified a parameter combination that reproduced the major flow characteristics of the observed 17–18 June 2024 debris flow. The final calibrated values of internal friction angle (δ), basal friction angle (ϕ_B), turbulent friction coefficient (ξ), and entrainment coefficient (C_E) were 17°, 9°, 10 m/s², and $10^{-5.55}$ kg⁻¹, respectively (Table 1). The calibrated simulation reproduced the observed runout extent and lateral confinement and captured the overall spatial transition from erosion and channel incision in the upper reaches to deposition downstream.

The following sections first compare the calibrated simulation with the observed geomorphic response and then examine the simulated spatial and temporal flow behaviour and the effects of turbulent friction and entrainment.

4.2.1 Comparison between observed and simulated geomorphic changes

The calibrated simulation was first compared with the observed geomorphic response derived from the DoD to assess how well the selected parameter combination reproduced the spatial pattern of erosion and deposition. The simulated and DoD-derived profiles show a broadly consistent longitudinal pattern of geomorphic change, with pronounced erosion in the upper and intermediate reaches followed by a transition toward deposition downstream (Fig. 8). The strongest erosion occurs within the upper approximately 400 m of the flow path, where the observed profile indicates erosion depths of approximately 15–18 m, locally approaching 19 m, compared with a maximum simulated incision of approximately 13 m. In the middle reach, both profiles show alternating erosion and

deposition features, although differences occur locally in their magnitude and position. Farther downstream, the two profiles show a transition toward predominantly deposition conditions, with relatively small elevation changes toward the end of the flow path.

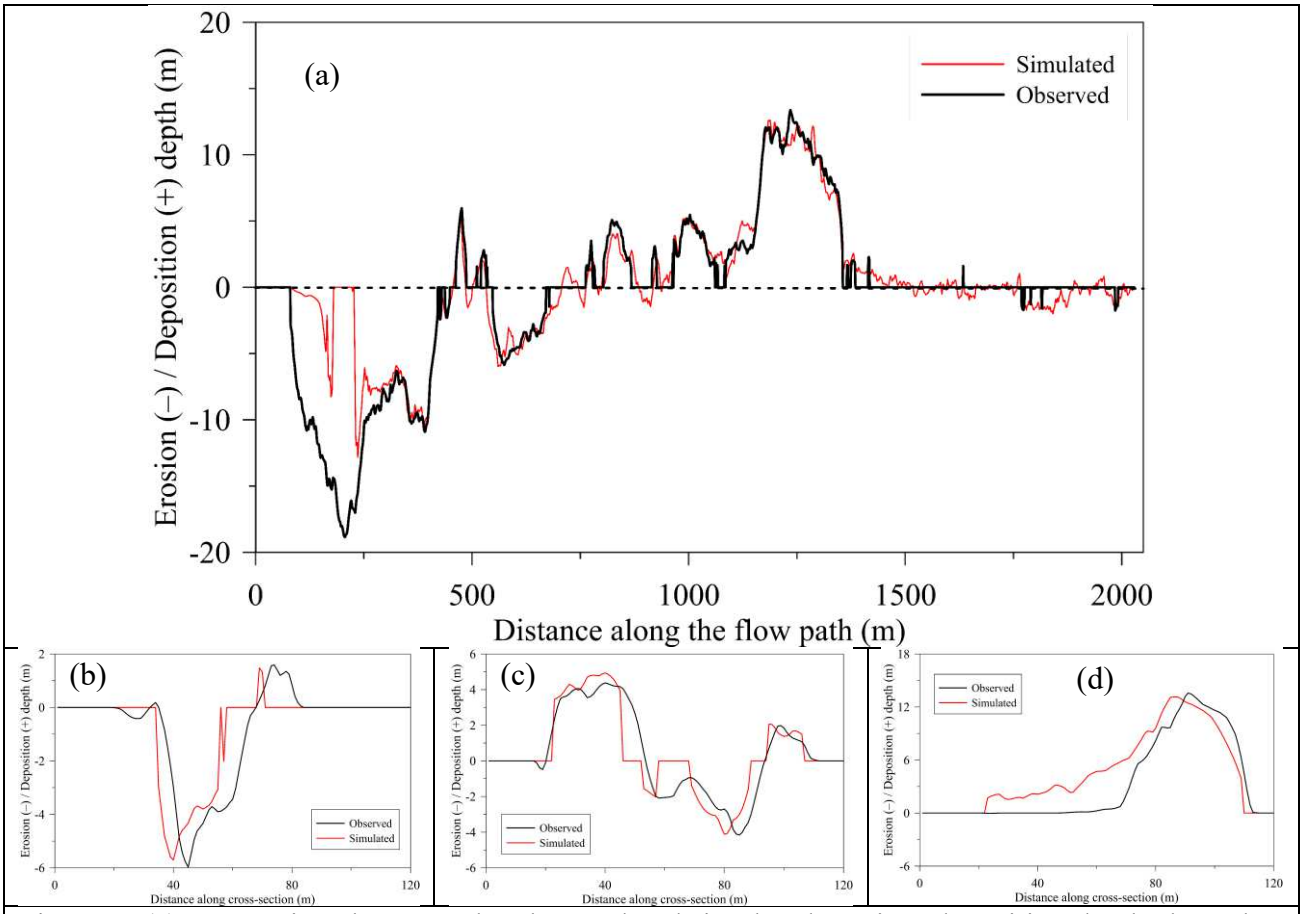


Figure 8: (a) Comparison between the observed and simulated erosion–deposition depth along the channel, (b) erosion and deposition at Section 1, (c) erosion and deposition at Section 2, and (d) deposition at Section 3.

At Section 1, the observed and simulated profiles show a similar erosion pattern, with the simulated profile slightly underestimating the depth of the initial incision (Fig. 8b). The overall shape of the erosion feature is nevertheless well represented, consistent with progressive entrainment during downstream propagation. At Section 2, both profiles show pronounced channel incision followed by a local deposition feature (Fig. 8c), with the simulated profile closely following the main form of the observed profile. At Section 3, the observed and simulated profiles show a similar transition toward deposition and a comparable deposition form (Fig. 8d), with the simulated profile generally reproducing the observed accumulation pattern.

Taken together, the longitudinal and cross-sectional comparisons indicate that the calibrated simulation reproduces the principal spatial evolution of the event, from erosion near the initiation area through channel incision to downstream deposition. The observed and simulated geomorphic patterns agree well, indicating that the calibrated parameter combination reproduces the main characteristics of the documented Longiarù event. Local differences in erosion and deposition magnitude may reflect

spatial variability in bed-material properties, small-scale topographic features, and limitations in representing event-scale release and entrainment processes. As the DoD-derived geomorphic response was used to constrain the calibration, this comparison represents an assessment of the calibrated model against the available geomorphic evidence rather than an independent validation.

4.2.2 Spatial distribution of simulated erosion and deposition

The simulation produced a distinct spatial pattern of erosion and deposition along the Seres Creek flow path (Fig.9a,b). Erosion was concentrated in the steep upper catchment and confined channel reaches, with the largest incision occurring near the initiation area, where simulated erosion locally reached approximately 14 m. Erosion zones were also prominent around channel bends and steeper channel segments, indicating continued bed-material removal along the transport corridor.

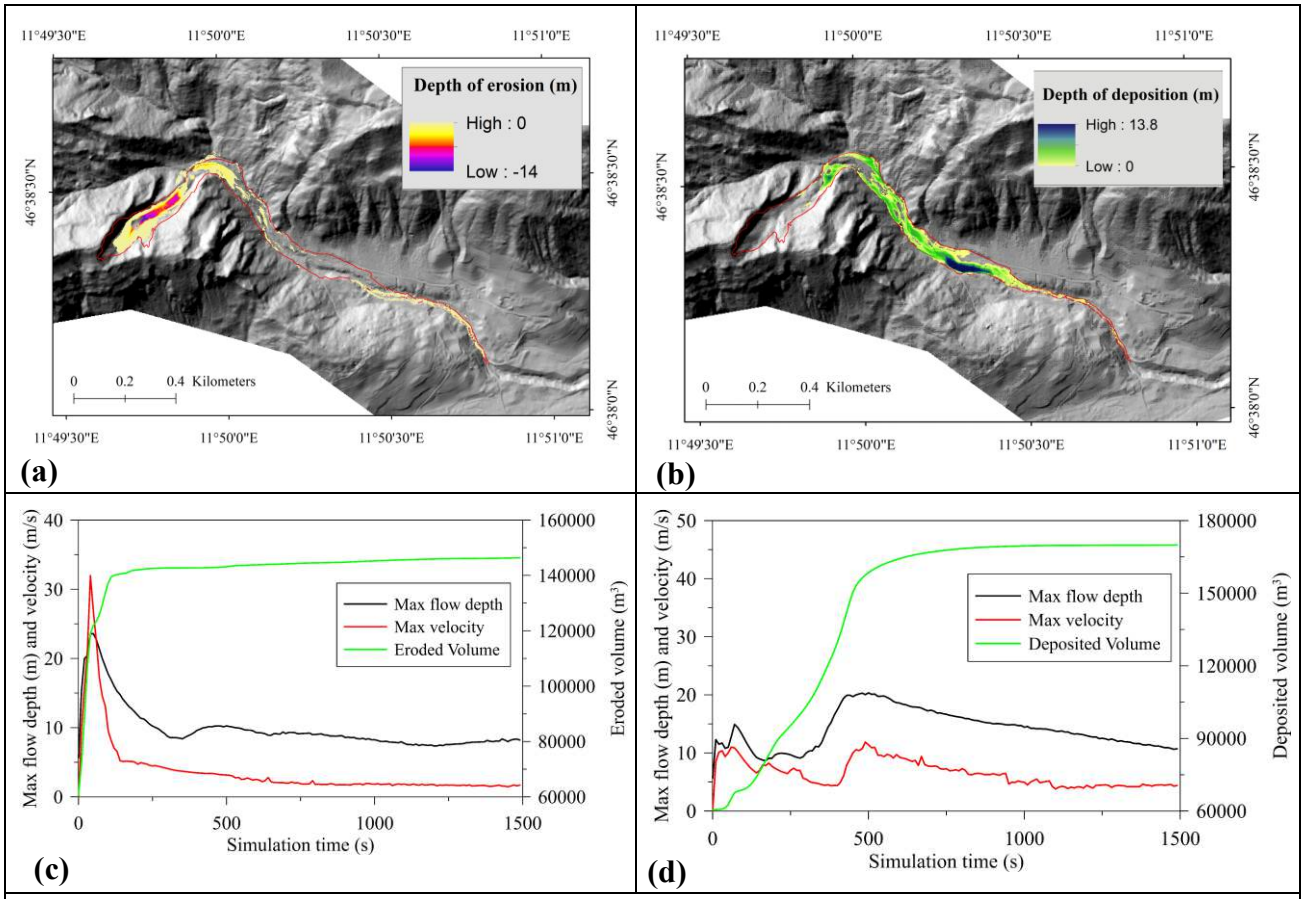


Figure 9: Simulated spatial distribution of (a) erosion and (b) deposition, and temporal evolution of maximum flow depth, velocity, and cumulative volumes of (c) erosion and (d) deposition for the 2024 Seres Creek debris flow under the calibrated friction and entrainment conditions ($\delta = 17°$, $\phi_B = 9°$, $\xi = 10$ m/s², and $C_E = 10^{-5.55}$ kg⁻¹).

Downstream, erosion progressively gave way to deposition as flow mobility decreased. The downstream deposition fan developed a lobate pattern, with simulated deposition reaching approximately 13.8 m in its proximal part and decreasing toward the distal margin. The simulation

reproduced the observed spatial transition from erosion in the initiation and transport reaches to deposition in the downstream fan, consistent with the pattern identified from the DoD analysis.

4.2.3 Temporal variation of flow parameters

Figures 9c and 9d show the temporal evolution of maximum flow depth and velocity together with cumulative erosion and deposition volumes during the calibrated simulation. The flow underwent a rapid initial acceleration, with maximum velocity increasing to approximately 30–35 m/s and maximum flow depth reaching approximately 8–10 m within the first 100 s. During this early stage, cumulative erosion increased rapidly as the high-energy flow entrained bed material while propagating downstream (Fig. 9c).

After approximately 100 s, maximum velocity decreased and generally remained within 5–10 m/s, while flow depth fluctuated as the moving mass interacted with the channel and continued to incorporate bed material. Cumulative erosion increased most rapidly during this stage before approaching a relatively stable value after approximately 250 s (Fig. 9c). In contrast, deposition became increasingly pronounced as the flow decelerated and entered lower-gradient reaches (Fig. 9d). The largest increase in cumulative deposited volume occurred between approximately 250 and 400 s, after which deposition progressively approached a stable value as the flow lost most of its transport capacity.

The temporal evolution therefore captures the progressive change from an initially energetic, erosion-dominated flow to a decelerating flow with increasing deposition, followed by final stabilization. This behaviour is consistent with the spatial transition from erosion-dominated upper and intermediate reaches to deposition on the downstream fan described in Section 4.2.2. As flow velocity was not directly measured in the field during the debris-flow event, the reported values therefore represent instantaneous spatial maxima that may occur locally and over short time intervals rather than velocities representative of the entire moving mass. Consequently, the simulated velocity magnitudes should be interpreted with greater caution than the runout extent and erosion–deposition pattern, which provided the primary geomorphic references for calibration.

4.2.4 Effect of turbulent friction on flow dynamics

The effect of turbulent friction on the simulated flow response was examined by comparing selected simulations with turbulent friction coefficients (ξ) of 8, 10, and 12 m/s^2 (Fig. 10). These values were selected from the broader range of 8–20 m/s^2 explored during the initial calibration, with $\xi = 10$ m/s^2 adopted as the calibrated value (Table 1). The comparison shows a clear change in flow mobility with increasing turbulent friction. At $\xi = 8$ m/s^2, the lower velocity-dependent resistance allowed greater preservation of flow momentum, resulting in higher velocities and deeper incision along steep channel segments. Increasing ξ to 10 and 12 m/s^2 progressively increased flow resistance and energy dissipation, leading to greater deceleration and a more localized distribution of erosion and deposition along the flow path. The higher-friction case also showed earlier attenuation of flow mobility and deposition.

The effect was also reflected in the temporal evolution of maximum velocity during both the erosion and deposition stages (Fig. 10a,b). The lower ξ case maintained higher velocities for longer, whereas

increasing ξ accelerated the reduction in flow velocity and promoted earlier deposition. The simulated value of $\xi = 10$ m/s^2 produced an intermediate flow response and reproduced the observed runout and spatial erosion–deposition pattern among the tested parameter combinations. The comparison demonstrates that turbulent friction exerts a clear control on simulated flow mobility and on the longitudinal transition from erosion to deposition. These results represent the response to the selected parameter values rather than a systematic exploration of the full range of ξ from 8 to 20 m/s^2.

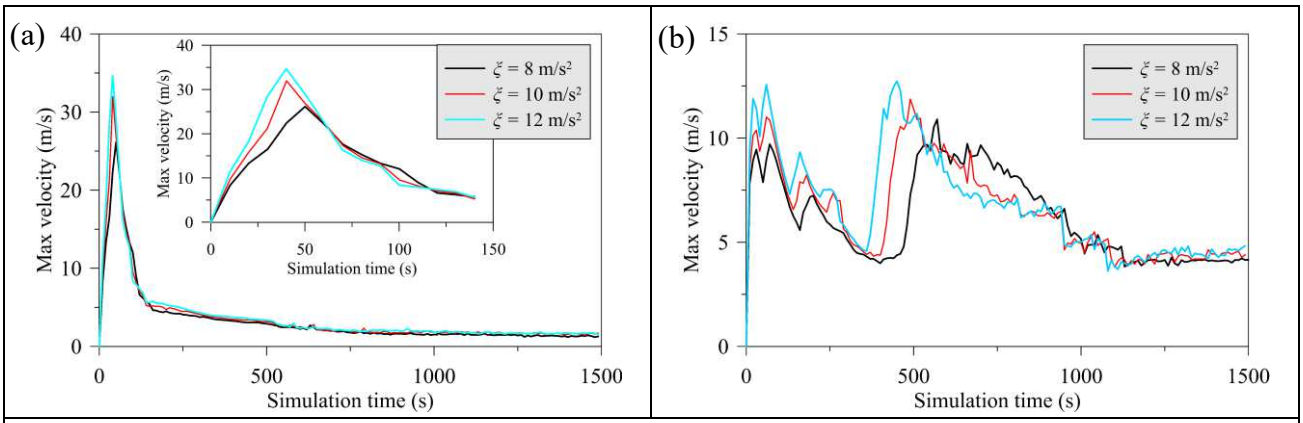


Figure 10: Effect of the turbulent friction parameter (ξ) on simulated maximum velocity during the (a) erosion and (b) deposition stages of the debris flow.

4.2.5 Effect of entrainment coefficient on flow dynamics

Figure 11 illustrates the effect of the entrainment coefficient (C_E) on the simulated velocity evolution during the erosion and deposition stages. The entrainment coefficient controls the rate at which bed material is incorporated into the moving mass and therefore affects the evolution of flow mass, momentum, and mobility. At lower C_E, relatively little bed material was incorporated into the moving mass, resulting in lower peak velocities and more rapid attenuation of the flow. Increasing C_E enhanced bed-material entrainment and increased the moving mass, allowing the flow to maintain its momentum for a longer period. Consequently, the higher entrainment cases exhibited greater peak velocities and a more prolonged dynamic phase during the erosion stage (Fig. 11a).

The effect of C_E persisted during the deposition stage (Fig. 11b). Higher entrainment coefficients delayed velocity attenuation and maintained flow mobility farther downstream, resulting in a downstream shift of the main deposition zone. In contrast, lower C_E values promoted earlier deceleration and deposition. The simulations with higher C_E also produced greater erosion, larger entrained volumes, and increased runout, indicating the importance of bed-material incorporation in maintaining flow mobility. The entrainment formulation used in r.avaflow relies on an empirical coefficient that requires calibration against observed flow behaviour and geomorphic change. The calibrated value of $C_E = 10^{-5.55}$ kg^{-1} should therefore be interpreted as an event-specific model parameter rather than a directly measured material property. In the present study, its value was constrained by the combined response of flow mobility and deposition location, together with the DoD-derived spatial pattern of erosion and deposition.

It should be noted that the entrainment formulation used in this study relies on an empirical coefficient that requires calibration against observed flow behaviour and geomorphic change. Consequently, the calibrated value should be regarded as an event-specific model parameter rather than a directly measured material property, and its applicability to other events or catchments may be limited. More mechanically based formulations that explicitly represent stress interactions and momentum exchange at the flow–bed interface may provide an avenue for reducing this dependence on empirical calibration in future modelling studies. In the present case of the Longiarù event, the observed differences in flow mobility and deposition location, together with the DoD-derived spatial pattern of erosion and deposition, provided the basis for constraining C_E to $10^{-5.55}$ kg^{-1}.

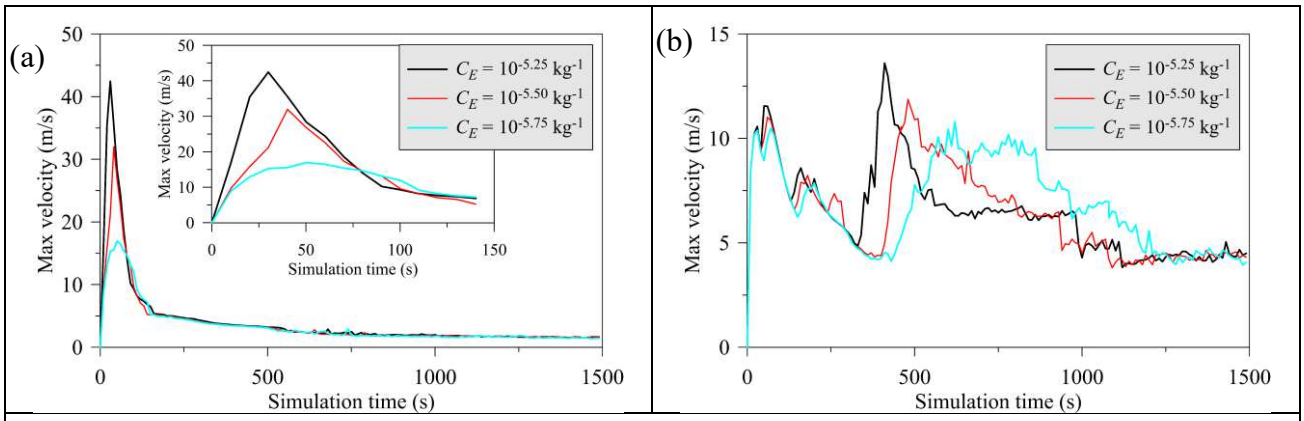


Figure 11: Effect of the entrainment coefficient (C_E) on simulated maximum velocity during the (a) erosion and (b) deposition stages of the debris flow.

5. Conclusions

The 17–18 June 2024 snowmelt-induced muddy debris flow in the Seres Creek catchment, Longiarù Valley, was characterized by a clear spatial transition from erosion in the initiation and transport reaches to deposition on the downstream fan. The DoD identified approximately 18,420 m³ of erosion and 16,850 m³ of deposition. The spatial distribution of geomorphic change provided constraints on the simulated flow response beyond runout extent alone, particularly for reproducing the transition from channel incision to downstream deposition.

The selected parameter combination of 17° internal friction, 9° basal friction, 10 m/s² turbulent friction, and $10^{-5.55}$ kg^{-1} entrainment reproduced the observed geomorphic response. The resulting simulation reproduced the major characteristics of the event, including the longitudinal transition from erosion and channel incision to downstream deposition. Comparisons among selected parameter values showed that turbulent friction had a strong effect on flow mobility and runout extent, whereas entrainment substantially influenced flow momentum, erosion, and the downstream position of deposition.

The simulated and DoD-derived geomorphic changes showed good spatial agreement along the main flow path and at the three representative cross-sections, with only localized differences in erosion and deposition magnitude. These results show that spatially distributed geomorphic change can provide constraints on frictional and entrainment parameters beyond runout extent alone, providing a spatially

informed basis for event-scale debris-flow modelling. Since the DoD-derived geomorphic response was used to constrain the model parameters, the comparison represents an assessment of the simulated event against the available geomorphic evidence rather than an independent validation.

The resulting parameter values should be regarded as event-specific constraints for the documented Longiarù event, and their transferability to other events or catchments remains to be established. Independent observations from additional debris-flow events and direct measurements of flow and material properties are needed to evaluate their broader applicability.

Funding

This study was carried out within the Space It Up project funded by the Italian Space Agency, ASI, and the Ministry of University and Research, MUR, under contract n. 2024-5-E.0 - CUP n. I53D24000060005. ED was supported by "Programma Fondo Europeo di Sviluppo Regionale (FESR) 2021-2027 della Provincia autonoma di Trento", CUP C65E25000120001.

Declaration of competing interests

The authors declare that they have no known competing financial interests or personal relationships that could have appeared to influence the work reported in this paper.

Data availability

The data that support the findings of this study are available from the corresponding author upon reasonable request.

Author contributions **Litan Dey:** Conceptualization, Methodology, Software, Formal analysis, Visualization, Writing – original draft. **Francesco Comiti:** Conceptualization, Methodology, Formal analysis, Writing – review & editing. **Martin Mergili:** Software, Validation, Writing – review & editing. **Pierpaolo Macconi:** Conceptualization, Methodology, Writing – review & editing. **Marco Cavalli:** Conceptualization, Methodology, Writing – review & editing. **Stefano Crema:** Conceptualization, Methodology, Writing – review & editing. **Eleonora Dallan:** Conceptualization, Methodology, Writing – review & editing. **Volkmar Mair:** Investigation, Data curation, Writing – review & editing. **Lukas Patscheider:** Investigation, Data curation, Writing – review & editing. **Marco Borga:** Conceptualization, Methodology, Formal analysis, Writing – review & editing.

References:

Anderson, S.W., 2019. Uncertainty in quantitative analyses of topographic change: error propagation and the role of thresholding. *Earth Surface Processes and Landforms* 44, 1015–1033.

Baggio, T., Mergili, M., D'Agostino, V., 2021. Advances in the simulation of debris flow erosion: The case study of the Rio Gere (Italy) event of the 4th August 2017. *Geomorphology* 381, 107664.

Berti, M., Simoni, A., 2005. Experimental evidences and numerical modelling of debris flow initiated by channel runoff. *Landslides* 2, 171–182.

Borga, M., Stoffel, M., Marchi, L., Marra, F., Jakob, M., 2014. Hydrogeomorphic response to extreme rainfall in headwater systems: Flash floods and debris flows. *Journal of Hydrology* 518, 194–205.

Brasington, J., Langham, J., Rumsby, B., 2003. Methodological sensitivity of morphometric estimates of coarse fluvial sediment transport. *Geomorphology* 53, 299–316.

Brasington, J., Rumsby, B.T., McVey, R.A., 2000. Monitoring and modelling morphological change in a braided gravel-bed river using high resolution GPS-based survey. *Earth Surface Processes and Landforms* 25, 973–990.

Cavalli, M., Goldin, B., Comiti, F., Brardinoni, F., Marchi, L., 2017. Assessment of erosion and deposition in steep mountain basins by differencing sequential digital terrain models. *Geomorphology* 291, 4–16.

Cavalli, M., Tarolli, P., 2011. Application of LiDAR technology for rivers analysis. *Italian Journal of Engineering Geology and Environment*, Special Issue 1, 33–44.

Crespi, A., Matiu, M., Bertoldi, G., Petitta, M., Zebisch, M., 2021. A high-resolution gridded dataset of daily temperature and precipitation records (1980–2018) for Trentino–South Tyrol (North-Eastern Italian Alps). *Earth System Science Data* 13, 2801–2818.

Cuomo, S., Pastor, M., Cascini, L., Castorino, G.C., 2014. Interplay of rheology and entrainment in debris avalanches: a numerical study. *Canadian Geotechnical Journal* 51, 1318–1330.

Dallan, E., Marchi, L., Rosatti, G., Zugliani, D., Cavalli, M., Crema, S., Valentinotti, R., Borga, M., 2025. What can be learnt from the catastrophic failure of a check dam system? A forensic analysis of a cascading natural-anthropogenic hazard. *Natural Hazards* 121, 12909–12931.

Dietrich, A., Krautblatter, M., 2019. Deciphering controls for debris-flow erosion derived from a LiDAR-recorded extreme event and a calibrated numerical model (Roßbichelbach, Germany). *Earth Surface Processes and Landforms* 44, 1346–1361.

Frank, F., McArdell, B.W., Huggel, C., Vieli, A., 2015. The importance of entrainment and bulking on debris flow runout modeling: examples from the Swiss Alps. *Natural Hazards and Earth System Sciences* 15, 2569–2583.

Fuller, I.C., Large, A.R., Charlton, M.E., Heritage, G.L., Milan, D.J., 2003. Reach-scale sediment transfers: an evaluation of two morphological budgeting approaches. *Earth Surface Processes and Landforms* 28, 889–903.

Gregoretti, C., Stancanelli, L.M., Bernard, M., Degetto, M., Boreggio, M., Lanzoni, S., 2019. Relevance of erosion processes when modelling in-channel gravel debris flows for efficient hazard assessment. *Journal of Hydrology* 568, 575–591.

Hungr, O., Leroueil, S., Picarelli, L., 2014. The Varnes classification of landslide types, an update. *Landslides* 11, 167–194.

Iverson, R.M., 1997. The physics of debris flows. *Reviews of Geophysics* 35, 245–296.

Iverson, R.M., 2014. Debris flows: behaviour and hazard assessment. *Geology Today* 30, 15–20.

Jakob, M., Hungr, O. (Eds.), 2005. *Debris-Flow Hazards and Related Phenomena*. Springer, Berlin.

Mergili, M., Fischer, J.-T., Krenn, J., Pudasaini, S.P., 2017. r.avaflow v1, an advanced open-source computational framework for the propagation and interaction of two-phase mass flows. *Geoscientific Model Development* 10, 553–569.

Mergili, M., Pfeffer, H., Kellerer-Pirklbauer, A., Zangerl, C., Pudasaini, S.P., 2025. r.avaflow v4, a multi-purpose landslide simulation framework. *Geoscientific Model Development* 18, 9879–9896.

Pastor, M., Haddad, B., Sorbino, G., Cuomo, S., Drempetic, V., 2009. A depth-integrated, coupled SPH model for flow-like landslides and related phenomena. *International Journal for Numerical and Analytical Methods in Geomechanics* 33, 143–172.

Pudasaini, S.P., Mergili, M., 2019. A multi-phase mass flow model. *Journal of Geophysical Research: Earth Surface* 124, 2920–2942.

Simoni, A., Bernard, M., Berti, M., Boreggio, M., Lanzoni, S., Stancanelli, L.M., Gregoretti, C., 2020. Runoff-generated debris flows: Observation of initiation conditions and erosion–deposition dynamics along the channel at Cancia (eastern Italian Alps). *Earth Surface Processes and Landforms* 45, 3556–3571.

Stoffel, M., Tiranti, D., Huggel, C., 2014. Climate change impacts on mass movements—case studies from the European Alps. *Science of the Total Environment* 493, 1255–1266.

Tai, Y.C., Noelle, S., Gray, J.M.N.T., Hutter, K., 2002. Shock-capturing and front-tracking methods for granular avalanches. *Journal of Computational Physics* 175, 269–301.

Takahashi, T., 2009. A review of Japanese debris flow research. *International Journal of Erosion Control Engineering* 2, 1–14.

Tiranti, D., Crema, S., Cavalli, M., Deangeli, C., 2019. An integrated study to evaluate debris flow hazard in Alpine environment. *Frontiers in Earth Science* 6, 60.

Varnes, D.J., 1978. Slope movement types and processes. In: Schuster, R.L., Krizek, R.J. (Eds.), *Landslides: Analysis and Control*, Special Report 176. Transportation Research Board, National Academy of Sciences, Washington, D.C., pp. 11–33.

Wang, Y., Hutter, K., Pudasaini, S.P., 2004. The Savage-Hutter theory: a system of partial differential equations for avalanche flows of snow, debris, and mud. *ZAMM—Journal of Applied Mathematics and Mechanics* 84, 507–527.

Wheaton, J.M., Brasington, J., Darby, S.E., Sear, D.A., 2010. Accounting for uncertainty in DEMs from repeat topographic surveys: improved sediment budgets. *Earth Surface Processes and Landforms* 35, 136–156.